Results in Physics 12 (2019) 943–946

Contents lists available at ScienceDirect

Results in Physics

journal homepage: www.elsevier.com/locate/rinp

MIMO multi-channels for simultaneous electro-optic distributed sensors

J. Ali[a], K. Chaiwong[b], N. Pornsuwancharoen[c], M.A. Jalil[d], I.S. Amiri[e], S. Punthawanunt[f], P. Youplao[g,h,*], P. Yupapin[g,h,*]

[a] Laser Centre, IBNU SINA ISIR, Universiti Teknologi Malaysia, 81310 Johor Bahru, Malaysia
[b] Department of Electrical and Electronics Engineering, Faculty of Industrial Technology, Loei Rajabhat University, Loei 42000, Thailand
[c] Department of Electrical Engineering, Faculty of Industry and Technology, Rajamangala University of Technology, Isan Sakon Nakhon Campus, 199 Phungkon, Sakon Nakhon 47160, Thailand
[d] Physics Department, Faculty of Science, Universiti Teknologi Malaysia, 81310 Johor Bahru, Malaysia
[e] Division of Materials Science and Engineering, Boston University, Boston, MA 02215, USA
[f] Multidisciplinary Research Center, Faculty of Science and Technology, Kasem Bundit University, Bangkok 10250, Thailand
[g] Computational Optics Research Group, Advanced Institute of Materials Science, Ton Duc Thang University, District 7, Ho Chi Minh City, Viet Nam
[h] Faculty of Applied Sciences, Ton Duc Thang University, District 7, Ho Chi Minh City, Viet Nam

A B S T R A C T

The distributed optical sensors using the multi-input light sources have been designed and simulated. It consists of 6 sensor nodes coupled to the main ring resonator, which is an optical circulator operation. It is a micro-scale device that can be fabricated by the current technology. The three distance light sources are simultaneously fed and the cross-connected signals combined in the circulator. By using the suitable parameters, the whispering gallery modes (WGMs) are generated at the center nodes from which the channel spacing signals can be obtained and used for distributed sensors. The analytical details and the simulation using the selected parameters are presented. The channel spacing of the cross-connected outputs of 1.2 μm is achieved. The simultaneous sensor sensitivity in the terms of $(\Delta\lambda/\lambda)$ of approximately 1.28 is obtained.

Introduction

Whispering gallery mode (WGM) of light with a microring resonator have been confirmed with a wide range of applications [1,2], which lead us to have more confidence in the realistic application. Up to date, there are many works have been theoretically proposed with the potential applications [3–8], where most of them use the microring resonator structure known as a panda-ring resonator. It is a nonlinear resonator that can provide the various advantages such as high-intensity pulse, short switching time and large free spectrum range (FSR). The most important is the WGM is available for free-space applications that can be used for light fidelity applications [9,10]. Moreover, the device ports are allowed the connection with the external functions, such as modulation, detection, filtering and multiplexing [11]. In this article, we have proposed the use of the optical circulator of the three light sources for the cross-connection, which is available for the multi-wavelength multiplexing and useful for LiFi link and communication for high traffic data communication. Another interesting application is that the circulation nodes are constructed by the panda-ring resonator, which can be employed as a sensor node of the distributed sensors, in which large area of sensor detection can be performed. The electro-optic signal conversion can also be available, which lead to the distributed sensors can be employed in both electrical and light signal applications. By using the stacked layers of silicon-graphene-gold called the plasmonic island [12], it is allowed the conversion of light and electrical signal conversion occurs. The proposed system is given in Fig. 1. Eqs. (1)–(3) representing the electrical output fields of the circuit [13]. The WGM field ($\mathbf{E_{WGM}}$) is given in the cylindrical coordinator [14]. The surface reflection of the reflector is neglected to simplify the equation, where $\mathbf{I_{WGMR}} = -\mathbf{R_{WGM}}\ \mathbf{I_{WGMR}}$. $\mathbf{R_{WGM}}$ is the reflection output. In case of the multi-input and output (MIMO) signal applications, the three-wavelength sources are input into the system and cross-connected source wavelengths are used to form the simultaneous multi-wavelength sensors, where the sensor heads are at the WGM outputs of each node.

The distributed sensors are formed by the large area of the sensors which can be coverage and simultaneous measurement. The used parameters are given in the captions of relevant figures.

Theoretical background

The MIMO system is shown in Fig. 1, where a selected light source is

* Corresponding authors at: Computational Optics Research Group, Advanced Institute of Materials Science, Ton Duc Thang University, District 7, Ho Chi Minh City, Viet Nam.
E-mail addresses: phichai.youplao@tdtu.edu.vn (P. Youplao), preecha.yupapin@tdtu.edu.vn (P. Yupapin).

https://doi.org/10.1016/j.rinp.2018.12.055
Received 15 June 2018; Received in revised form 28 November 2018; Accepted 11 December 2018
Available online 15 December 2018

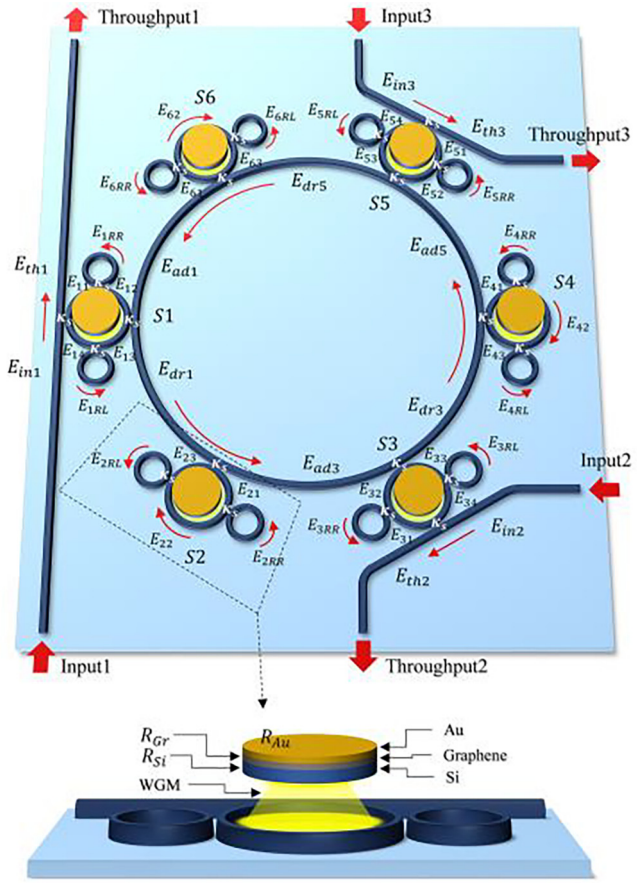

Fig. 1. Schematic of a plasmonic island structure, where E_{in}, E_{th}, E_{dr}, E_{ad} are the electrical fields of the input, through, drop and add ports, R_R, R_L, and R_D are the right, the left, and the centre ring, respectively, κ_s: the coupling coefficients are 0.5. R_{Si}: Silicon circle radius, R_{Gr}: Graphene circle radius, and R_{Au}: Gold sphere radius.

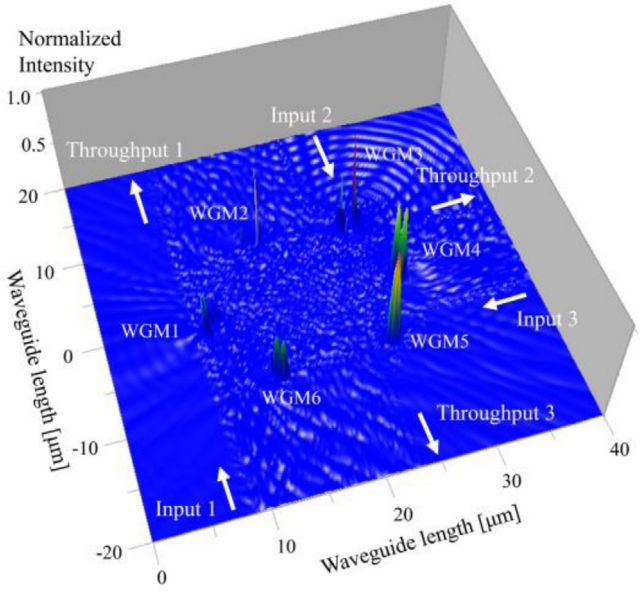

Fig. 2. WGM outputs, where the input light source power is 10 mW with a wavelength center is at 1.55 μm. The ring system, $R_L = R_R = 0.5$ μm, $R_D = 1.0$ μm. Each the coupling constant, $\kappa_s = 0.5$, the ring material is the ***InGaAsP/InP***, of which the refractive index; $n_0 = 3.14$, $n_2 = 1.3 \times 10^{-17}\ m^2\,W^{-1}$. The waveguide loss is 0.1 dBmm^{-1}, the effective core area is 0.50 μm^2.

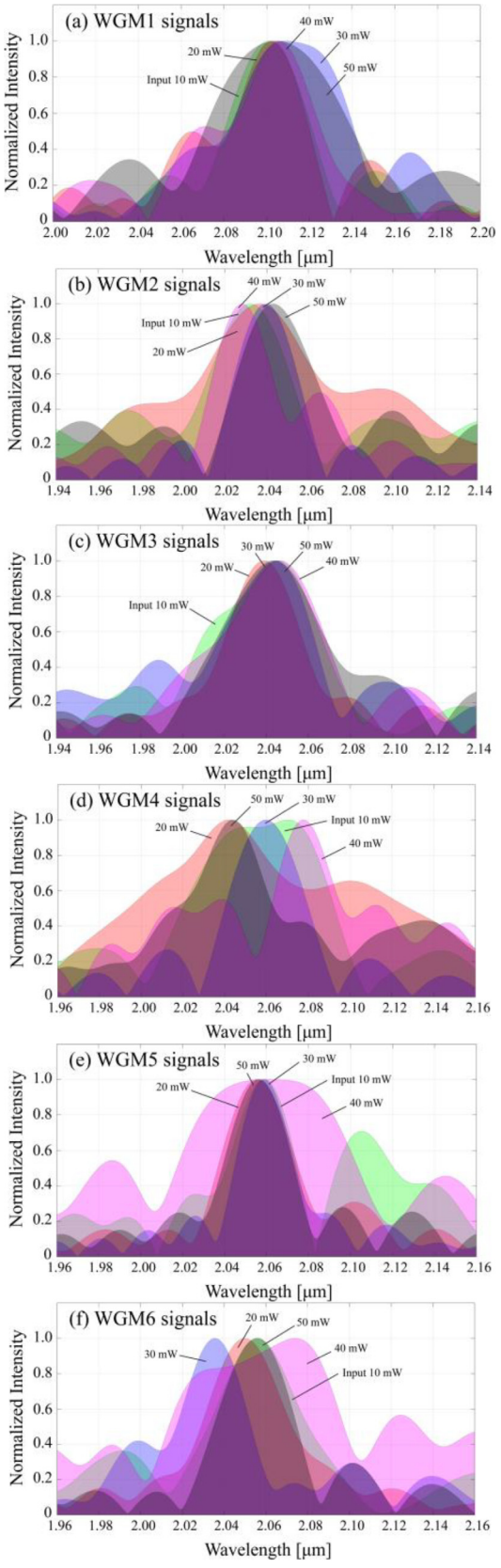

Fig. 3. Plot of the WGM outputs of the distributed sensor nodes, where the input power was changed from 10 to 50 mW. The different WGM of the different optical paths are seen and distinguished, which can be configured to be the shift in OPDs and the center WGMs.

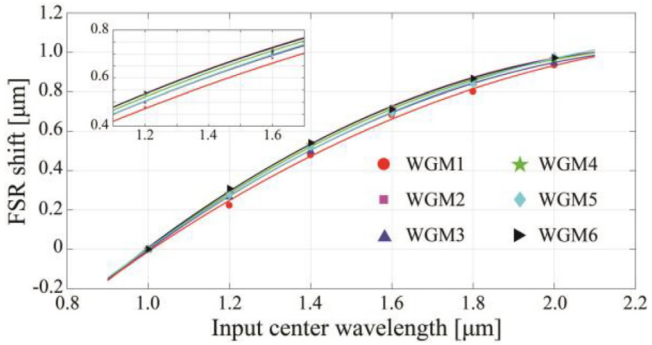

Fig. 4. The shift in the WGM of each node is the sensor sensitivity, which is $(\Delta\lambda/\lambda) \approx \frac{0.2563}{0.2} = \mathbf{1.2815}$ of the six-point distributed sensors at the WGM outputs, where the input light power is fixed at 10 mW.

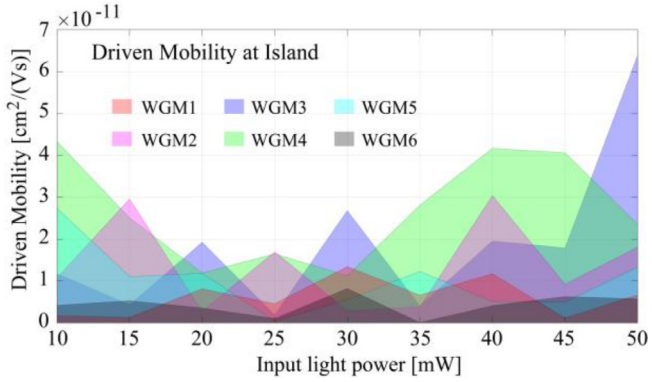

Fig. 5. Plot of mobility output of the six-point distributed sensors at the plasmonic island, where the parameters are: $\boldsymbol{R_{Si} = R_{Gr} = R_{Au}}$= 800 nm, the thickness of each layer, Si, Graphene, and Gold, is 0.2 μm, 0.1 μm, and 0.1 μm, respectively. The maximum mobility output of is $cm^2\ (Vs)^{-1}$obtained, with the input power is varied from 10 to 50 mW.

fed into the system via an input port, which is represented as the input electric field ($\boldsymbol{E_{in}}$). The input light beams are in the forms of the different source input with the same wavelength. The input light beams are in the forms of the different source input with the same wavelength. This input electric field is fed into the z-axis and circulated within the system, described by the equations, where $\boldsymbol{E_{in} = E_Z = E_0 e^{-ik_z - \omega t + \varphi}}$, $\boldsymbol{E_0}$ is the initial electric field amplitude (real), $\boldsymbol{k_z}$ is the wave number in the direction of propagation (z-axis), ω is the angular frequency, and φ is the phase of light. The distributed electrical fields, within the MIMO system, are given as the following details.

$$\boldsymbol{E_{th_1} = \left[\frac{G.\,F^2 - G.\,F.\,C - A.\,H.\,J}{F^2.\,J - C.\,F.\,J}\right] E_{in_1} + \left[\frac{(F.\,I - B.\,H - C.\,I)}{F.\,(F - C)}\right] E_{ad_1}} \tag{1}$$

$$\boldsymbol{E_{dr_1} = \frac{K(F - C - BL/K)E_{ad_1} - L.\,A.\,E_{in_1}}{M(F - C)}} \tag{2}$$

$$\boldsymbol{E_{ad_1} = E_{dr_5}(\sqrt{1-\kappa}) - \sqrt{\kappa}^2\left(\frac{S}{S - T}\right)} \tag{3}$$

where the parameters of nodes 1,3,5 are given by

$$\boldsymbol{A} = [x_1 z_1 PL_8 - x_1 z_1 x_2 y_2 P_1 PL_8 - x_1 z_1 x_4 y_4 P_2 PL_8 + x_1 z_1 x_2 y_2 x_4 y_4 P_1 P_2 PL_8]$$

$$\boldsymbol{B} = [x_1 y_1 x_3 z_3 x_4 y_4 PL_4 PL_8 - x_1 y_1 x_2 y_2 x_3 z_3 x_4 y_4 P_1 PL_4 PL_8 - x_1 y_1 x_3 z_3 x_4^2 y_4^2 P_2 PL_4 PL_8 + x_1 y_1 x_2 y_2 x_3 z_3 x_4^2 y_4^2 P_1 P_2 PL_8 PL_4 - x_1 y_1 x_3 z_3 x_4^2 z_4^2 P_2 PL_4 PL_8 + x_1 y_1 x_2 y_2 x_3 z_3 x_4^2 z_4^2 P_1 P_2 PL_4 PL_8]$$

$$\boldsymbol{C} = [x_1 y_1 x_2 y_2 x_3 y_3 x_4 y_4 (PL_4)^2 - x_1 y_1 x_2^2 y_2^2 x_3 y_3 x_4 y_4 P_1 (PL_4)^2 - x_1 y_1 x_2^2 z_2^2 x_3 y_3 x_4 y_4 P_1 (PL_4)^2 - x_1 y_1 x_2 y_2 x_3 y_3 x_4^2 y_4^2 P_2 (PL_4)^2 + x_1 y_1 x_2^2 y_2^2 x_3 y_3 x_4^2 y_4^2 P_1 P_2 (PL_4)^2 + x_1 y_1 x_2^2 z_2^2 x_3 y_3 x_4^2 y_4^2 P_1 P_2 (PL_4)^2 - x_1 y_1 x_2 y_2 x_3 y_3 x_4^2 z_4^2 P_2 (PL_4)^2 + x_1 y_1 x_2^2 y_2^2 x_3 y_3 x_4^2 z_4^2 P_1 P_2 (PL_4)^2 + x_1 y_1 x_2^2 z_2^2 x_3 y_3 x_4^2 z_4^2 P_1 P_2 (PL_4)^2]$$

$$\boldsymbol{F} = [1 - x_2 y_2 P_1 - x_4 y_4 P_2 + x_2 y_2 x_4 y_4 P_1 P_2],\ \boldsymbol{G} = [x_1 y_1 - x_1 x_4 y_1 y_4 P_2]$$

$$\boldsymbol{H} = j[x_1 x_2 x_3 x_4 y_2 y_3 y_4 z_1 . PL_4 PL_8 - x_4^2 y_4^2 x_1 x_2 x_3 y_2 y_3 z_1 . P_2 PL_4 PL_8 - x_4^2 z_4^2 x_1 x_2 x_3 y_2 y_3 z_1 . P_2 PL_4 PL_8 - x_2^2 y_2^2 x_1 x_3 x_4 y_3 y_4 z_1 . P_1 PL_4 PL_8 + x_2^2 x_4^2 y_2^2 y_4^2 x_1 x_3 y_3 z_1 . P_1 P_2 PL_4 PL_8 + x_2^2 x_4^2 y_2^2 z_4^2 x_1 x_3 y_3 z_1 P_1 P_2 . PL_4 PL_8 - x_2^2 z_2^2 x_1 x_4 x_3 y_3 y_4 z_1 . P_1 PL_4 PL_8 + x_2^2 x_4^2 z_2^2 y_4^2 x_1 x_3 y_3 z_1 . P_1 P_2 PL_4 PL_8 + x_2^2 x_4^2 z_2^2 z_4^2 x_1 x_3 y_3 z_1 . P_1 P_2 PL_4 PL_8]$$

$$\boldsymbol{I} = -[x_1 x_3 x_4 y_4 z_1 z_3 PL_8^2 - x_4^2 y_4^2 x_1 x_3 z_1 z_3 P_2 PL_8^2 - x_4^2 z_4^2 x_1 x_3 z_1 z_3 P_2 PL_8^2 - x_1 x_2 x_3 x_4 z_1 z_3 y_2 y_4 P_1 PL_8^2 + x_4^2 y_4^2 x_1 x_2 x_3 y_2 z_1 z_3 P_1 P_2 PL_8^2 + x_4^2 z_4^2 x_1 x_2 x_3 y_2 z_1 z_3 P_1 P_2 PL_8^2]$$

$$\boldsymbol{J} = [1 - x_4 y_4 P_2],\ \boldsymbol{K} = [x_3 y_3 (1 - x_2 y_2 P_1)],\ \boldsymbol{L} = [x_2 x_3 y_2 z_3 PL_8 - x_2^2 y_2^2 x_3 z_3 P_1 PL_8 - x_2^2 z_2^2 x_3 z_3 P_1 PL_8],\ \boldsymbol{M} = [1 - x_2 y_2 P_1]$$

where the parameters of nodes 2, 4, 6 are given by

$$\boldsymbol{S} = [x_1 y_1 x_2 y_2 x_3 y_3 - x_1 y_1 x_2 y_2 x_3^2 y_3^2 P_2 - x_1 y_1 x_2 y_2 x_2^2 z_3^2 P_2 - x_1 y_1 x_2^2 y_2^2 x_3 y_3 P_1 + x_1 y_1 x_2^2 y_2^2 x_3^2 y_3^2 P_1 P_2 + x_1 y_1 x_2^2 y_2^2 x_2^2 z_3^2 P_1 P_2 - x_1 y_1 x_3 y_3 x_2^2 z_2^2 + x_1 y_1 x_3^2 y_3^2 x_2^2 z_2^2 P_2 + x_1 y_1 x_2^2 z_2^2 x_3^2 z_3^2 P_2] PL_8$$

$$T = 1 - x_2 y_2 P_1 - x_3 y_3 P_2 + x_2 y_2 x_3 y_3 P_1 P_2$$

$x_i = \sqrt{1-\gamma_i}$, $y_i = \sqrt{1-\kappa_i}$, $z_i = \sqrt{\kappa_i}$, where i = 1,2, 3,4.

$P_1 = e^{-\frac{\alpha}{2}L_R - jk_n L_R}$, $P_2 = e^{-\frac{\alpha}{2}L_L - jk_n L_L}$: $L_R = 2\pi R_R$, $L_L = 2\pi R_L$

$PL_2 = e^{-\frac{\alpha}{2}L_D - jk_n L_D}$, $PL_4 = e^{-\frac{\alpha}{2}\frac{L_D}{2} - jk_n \frac{L_D}{2}}$: $PL_8 = e^{-\frac{\alpha}{2}\frac{L_D}{4} - jk_n \frac{L_D}{4}}$

and

$$E_{th_2} = \left[\frac{G.\,F^2 - G.\,F.\,C - A.\,H.\,J}{F^2.\,J - C.\,F.\,J}\right] E_{in_2} + \left[\frac{(F.\,I - B.\,H - C.\,I)}{F.\,(F - C)}\right] E_{ad_3}$$

$$E_{dr_3} = \frac{K(F - C - BL/K)E_{ad_3} - L.\,A.\,E_{in_2}}{M(F - C)}$$

$$E_{ad_3} = E_{dr_1}\left(\sqrt{1-\kappa} - \sqrt{\kappa}^2\left(\frac{Q}{S - T}\right)\right)$$

$$E_{th_3} = \left[\frac{G.\,F^2 - G.\,F.\,C - A.\,H.\,J}{F^2.\,J - C.\,F.\,J}\right] E_{in_3} + \left[\frac{(F.\,I - B.\,H - C.\,I)}{F.\,(F - C)}\right] E_{ad_5}$$

$$E_{dr_5} = \frac{K(F - C - BL/K)E_{ad_5} - L.\,A.\,E_{in_3}}{M(F - C)}$$

$$E_{ad_5} = E_{dr_3}(\sqrt{1-\kappa} - \sqrt{\kappa}^2\left(\frac{Q}{S - T}\right)$$

Simulation results

In a simulation, the graphical approach known as an Optiwave program was used to specify the suitable parameters, from which the results are plotted in Fig. 2. In the simulation, the same light source is input into the circulator via the input port of the three different nodes

(Panda-ring resonators). Light power from the different directions is coupled into the selected node and circulated in the optical circulator, in which each the output is obtained at each the throughput port. The resonant WGMs of the different channels are seen at the node centers which are the reference signals of the distributed sensors. The changes in the environment, such as temperature variations on the interested surface, cause the change in the refractive index, which can be measured in term of the change in the wavelength relative to the reference position.

By using the practical parameters [15–17], the used numerical tools were the Optiwave and MATLAB programs. Fig. 2 shows the WGM outputs of all nodes, where the input light source power is 10 mW, with a wavelength center is at 1.55 μm. The ring system, $\boldsymbol{R_L} = \boldsymbol{R_R} = 0.5\,\mu m$, $\boldsymbol{R_D} = 1.0\,\mu m$. Each the coupling constant, $\boldsymbol{\kappa_s} = 0.5$, the ring material is the ***InGaAsPIn-P***, of which the refractive index$\boldsymbol{n_0} = 3.14$, $\boldsymbol{n_2} = 1.3 \times 10^{-17}\,m^2\,W^{-1}$, where the selected parameters are used in the simulation.

The plot of the change in the input power from 10 to 50 mW is shown in Fig. 3. The change in the WGM wavelength due to the change in the input power is shown in the Figure, where the calculation sensor sensitivity in terms of $(\Delta\boldsymbol{\lambda}/\boldsymbol{\lambda}) \approx \frac{0.2563}{0.2} = 1.2815$ of the six-point distributed sensors at the WGM outputs is obtained, where the input light power is 10 mW. Such a sensor system can also be applied by the electrical inputs by the conversion between the light intensity and the electron mobility, which means that the connection with the electrical device is available (Fig. 4 and 5).

The plot of mobility output of the six-point distributed sensors at the plasmonic island, where the parameters are $\boldsymbol{R_{Si}} = \boldsymbol{R_{Gr}} = \boldsymbol{R_{Au}} = 800\,nm$, the thickness of each layer are Si, Graphene, and Gold is 0.2 μm, 0.1 μm, and 0.1 μm, respectively. In the calculation, the electron mobility, $\boldsymbol{\mu} = \frac{\boldsymbol{V_d}}{\boldsymbol{E}}$, where $\boldsymbol{V_d}$ is Drift velocity, which is $\boldsymbol{v_d} = \frac{\boldsymbol{j_s}}{\boldsymbol{nq}}$, where $\boldsymbol{j_s} = \boldsymbol{\sigma LE}$ is the current density flowing through the material, L is the material length (thickness), and $\boldsymbol{n}$ is the charge-carrier number density (electrons per cubic meter). The charge-carrier number density, $\boldsymbol{n}$ = [Density × free electron number per atom × Avogadro's constant]/[Molar mass] electrons per cubic meter. For Au, the density is $19.32\,g\,cm^{-3}$, the Avogadro's constant is 6.02×10^{23} atoms, the free electron number is 1, the Molar mass is $196.967\,gmol^{-1}$, and the conductivity, $\sigma = 4.10 \times 10^{7}\,Sm^{-1}$ [15–17].

Conclusion

The MIMO of the optical circulator system is proposed to perform the multi-channel distributed sensor application. The large area sensors can be formed by such a device, from which the sensor network among the sensor nodes can be formed by the WGM outputs. The change in the WGM wavelengths can be measured with respected to the reference. The proposed system has the capability of self-calibration. The series of the WGM signals are obtained at the through ports, which can be distinguished by the different location (device length). The results have shown that the sensor sensitivity in terms of (Δλ/λ) approximately of 1.28 is obtained. In applications, such a device can be used to form the optical circulator for traffic management. The maximum mobility output of $cm^2(Vs)^{-1}$ is obtained, with the input power is varied from 10 to 50 mW. Moreover, the sensor nodes are simultaneously operated that can be used to form the micro-network for bio-cells communication. From which each node is placed by the different molecule or cells, from which the change in the sensor signals from each node can be measured and cell location identified [18].

Acknowledgment

The authors would like to give the appreciation for the research financial support and the research facilities and financial support from the Universiti Teknologi Malaysia, Johor Bahru, Malaysia through Flagship UTM shine project (03G82), Tier 1 (16H44) and Tier 2 (15 J57) grants.

Appendix A. Supplementary data

Supplementary data to this article can be found online at https://doi.org/10.1016/j.rinp.2018.12.055.

References

[1] Wolverton M. Whispering resonances to the terahertz regime. AIP Scilight 2018. https://doi.org/10.1063/1.5024669.
[2] Vogt DW, Leonhardt R. Ultra-high Q terahertz whispering-gallery modes in a silicon resonator. APL Photonics 2018;3:051702.
[3] Sarapat N, Frank TD, Yupapin PP. Conjugate mirror design and simulation using a nonlinear coupling microring circuit. J Nonlinear Opt Phys Mater 2013;22(3):1–11.
[4] Yothapakdee K, Yupapin PP, Tamee K. Brain signal monitoring model using THz whispering gallery modes generated by micro-conjugate mirror probe. J IFSA Sens Transducers 2015;186(3):112–7.
[5] Ali J, Youplao P, Pornsuwancharoen N, Aziz MS, Chiangga S, Amiri IS, et al. On-chip remote charger model using plasmonic island circuit. Results Phys 2018;9:815–8.
[6] Ali J, Pornsuwancharoen N, Youplao P, Aziz MS, Amiri IS, Chaiwong K, et al. Coherent light squeezing states within a modified microring system. Results Phys 2018;9:211–4.
[7] Pornsuwancharoen N, Youplao P, Aziz MS, Ali J, Amiri IS, Punthawanunt S, et al. In-situ 3D micro-sensor model using embedded plasmonic island for biosensors. Microsyst Technol 2018;24(9):3631–5.
[8] Pornsuwancharoen N, Youplao P, Chaiwong K, Phatharacorn P, Chiangga S, Koledov V, et al. Manual control of optical tweezer switching for particle trapping and injection. IET Micro Nano Lett 2018;13(7):911–4.
[9] Ali J, Youplao P, Pornsuwancharoen N, et al. On-chip remote charger model using plasmonic island circuit. Results Phys 2018;9:815–8.
[10] Punthawanunt S, Aziz MS, Phatharacorn P, Chiangga S, Ali J, Yupapin P. LiFi cross-connection node model using whispering gallery mode of light in a microring resonator. Microsyst Technol 2018;24(12):4833–8.
[11] Ali J, Youplao P, Pornsuwancharoen N, Jalil MA, Chaiwong K, Aziz MS, et al. On-chip electro-optic multiplexing circuit using serial microring boxcar filters. Results Phys 2018;10:18–21.
[12] Pornsuwancharoen N, Amiri IS, Suhailin F, Aziz MS, Ali J, Singh G, et al. Micro-current source generated by a WGM of light within a stacked silicon-graphene-Au waveguide. IEEE Photonics Technol Lett 2017;29:1768–71.
[13] Soysouvanh S, Jalil M, Amiri IS, et al. Ultra-fast electro-optic switching control using a soliton pulse within a modified add-drop multiplexer. Microsyst Technol 2018;24(9):3777–82.
[14] Phatharacorn P, Chiangga S, Yupapin P. Analytical and simulation results of a triple micro whispering gallery mode probe system for a 3D blood flow rate sensor. Appl Opt 2019;55(33):009504.
[15] Atabaki AH, Moazenni S, Pavanello F, et al. Integrating photonics with silicon nanoelectronics for next generation of system on a chip. Nature 2018;556:349–54.
[16] Koos C, Jacome L, Poulton C, et al. Nonlinear silicon-on-insulator waveguides for all-optical signal processing. Opt Express 2007;15:5976–90.
[17] Mohr PJ, Newell DB, Taylor BN. CODATA recommended values of the fundamental physical constants 2014. Rev Mod Phys 2016;88. 035009-1-73.
[18] Youplao P, Pornsuwancharoen N, Amiri IS, Jalil MA, Aziz MS, Ali J, et al. Microring stereo sensor model using kerr-vernier effect for bio-cell sensor and communication. Nano Commun Networks 2018;17:30–5.